PNAS

Supporting Information for

Demographic models predict end-Pleistocene arrival and rapid expansion of pre-agropastoralist humans in Cyprus

Corey J. A. Bradshaw, Christian Reepmeyer, Frédérik Saltré, Athos Agapiou, Vasiliki Kassianidou, Stella Demesticha, Zomenia Zomeni, Miltiadis Polidorou, Theodora Moutsiou

Corresponding authors: Corey J. A. Bradshaw; Dora Moutsiou
Email: corey.bradshaw@flinders.edu.au; moutsiou.theodora@ucy.ac.cy

This PDF file includes:

Appendix I

Fig. S1. HadCM3 (1) hindcasts of anomalies of net primary production (NPP; green), temperature (red), and precipitation (blue) for Cyprus, with the CRIWM-estimated human arrival window shown in vertical grey, the Bølling-Allerød interstadial (B-O; light pink shading), the Younger Dryas (light blue shading), and the early Holocene (brown shading). The end of the Last Glacial Maximum (LGM) is indicated in light blue shading.

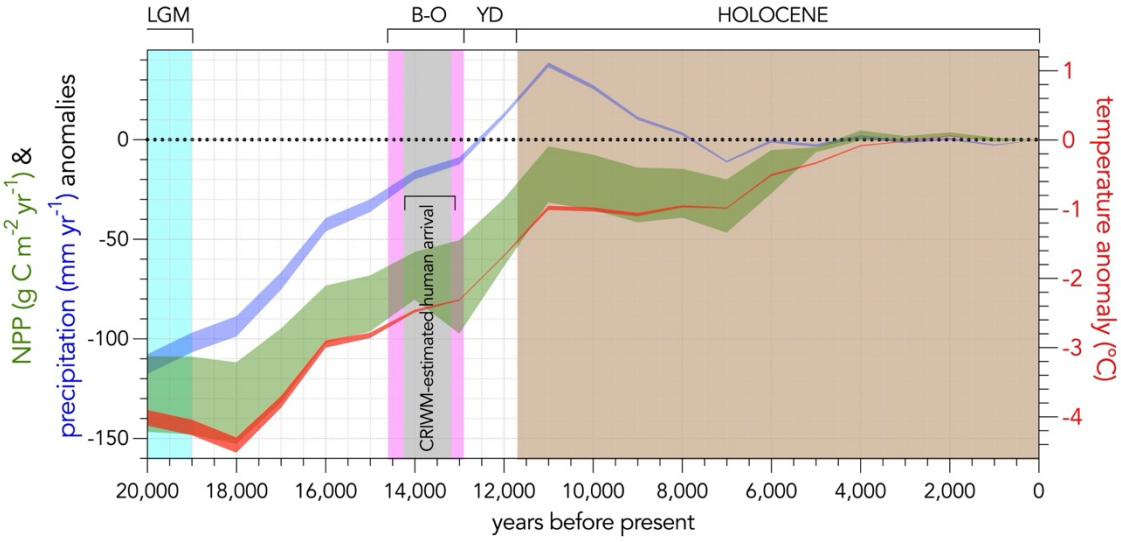

Fig. S2. Hindcasted net primary production (green scale) from the HadCM3 global circulation model (1) at 14 ka for the Eastern Mediterranean-Middle East (resolution 0.5º × 0.5º latitude/longitude). The model predicts a net primary production of the cells covering Cyprus ranging from 181–223 g C m^{-2} $year^{-1}$, whereas other sites with dated archaeological material around 14 ka on the mainland (e.g., Karain and Öküzini Caves, Türkiye; Moghr El Ahwal Cave 3, Lebanon; Hayonim Terrace and Kebara Cave, Israel — Palmisano et al. 2022) have hindcasted net primary production ranging from 140 to 216 g C m^{-2} $year^{-1}$. Background blue indicates relative bathymetry in the Mediterranean Sea.

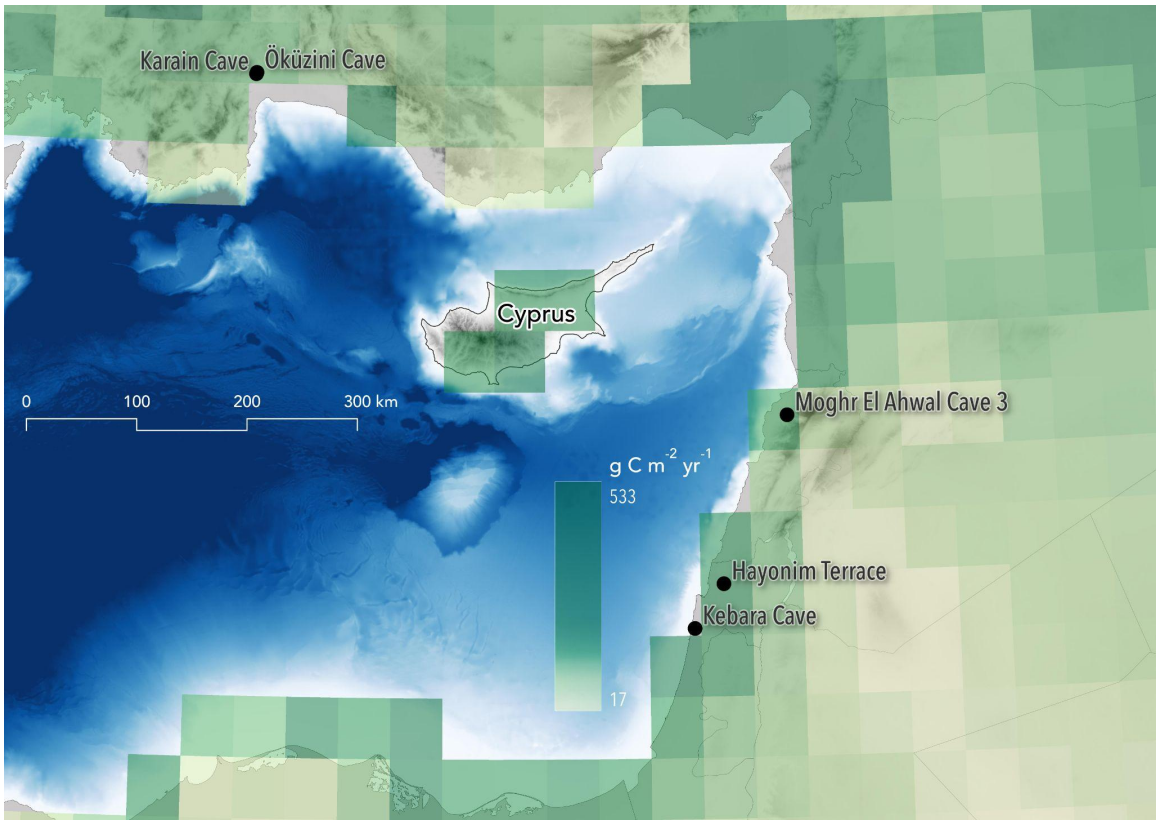

Fig. S3. Comparison of hindcasted temperature anomalies (ºC) derived from the HadCM3 (1) and TraCE21ka (2, 3) global circulation models. The temporally finer-resolution TraCE21 (seamless, but shown here in 100-year increments) compared to HadCM3 (1000 years) captures the dynamics of the Bølling-Allerød interstadial (B-O; light pink shading) and the Younger Dryas (light blue shading) compared to other climate hindcasts (4). Also shown is the end of the Last Glacial Maximum (LGM) in light blue shading.

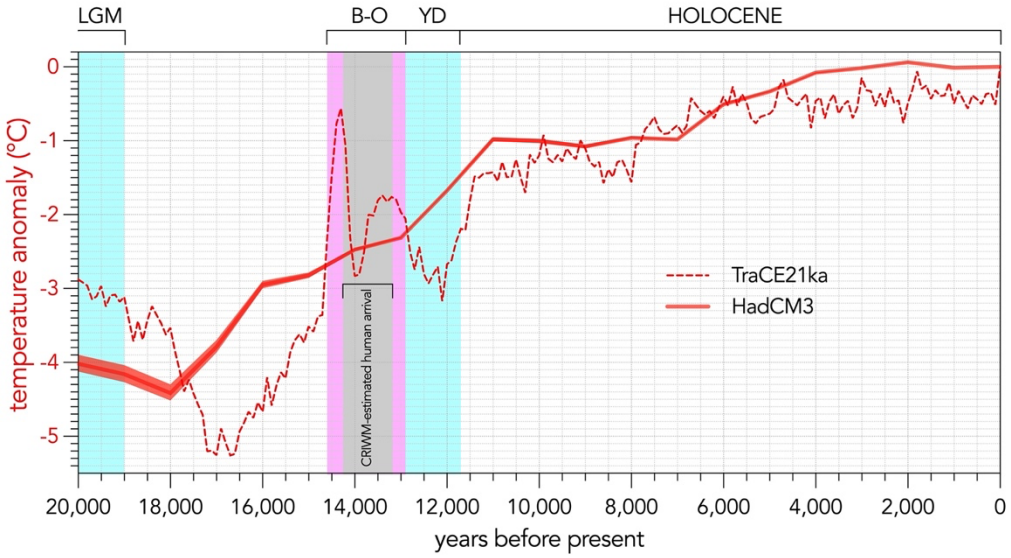

Estimates of hunter-gatherer densities standardized to persons km^{-2}

Obtaining estimates of pre-agropastoral human densities from the literature (5-12), we first standardized all values to persons km^{-2}. We then developed a bootstrapping approach to estimate the 95% confidence intervals of median density across all values, and for those pertaining only to the Mediterranean and Levant/Near East region (using the script `densities` available at github.com/cjabradshaw/CyprusHumanPleistocene/scripts).

The 95% confidence interval of the median human density across all values listed in Table S1 was 0.045 to 0.433 people km^{-2}, and for the six estimates pertaining to the Mediterranean and Levant/Near East, the confidence interval was 0.129 to 1.324 people km^{-2}.

Table S1. Estimated and modelled human population densities for pre-agropastoral societies from Europe to the Near East standardized to persons km^{-2}. 1 ka = 1,000 calendar years before present.

Period	Region	persons km^{-2}	Type	Reference
Modern Era	global	0.034	terrestrial animal subsistence	Binford (2001)
Modern Era	Levant	0.01	technology-unaided hunter-gatherer	Binford (2001)
Upper Palaeolithic	Europe	0.0017	mean	Bocquet-Appel et al. (2005)
Late Natufian (12.5 ka–12.0 ka)	Near East	0.9–2.95	mean	Coward & Dunbar (2014)
Pre-pottery Neolithic (12.0 ka–10.5 ka)	Near East	0.4072–1.328	mean	Coward & Dunbar (2014)
10 ka	Eastern Mediterranean	0.03–0.11	potential	Kavanagh et al. (2018)
12 ka	Fertile Crescent	0.5	potential	Kavanagh et al. (2018)
Late glacial final Palaeolithic	southern Scandinavia	0.002–0.003	overall mean	Lundström et al. (2021)
Late glacial final Palaeolithic	southern Scandinavia	0.02–0.05	core area	Lundström et al. (2021)
Late glacial final Palaeolithic	southern Scandinavia	0.09–0.28	home range	Lundström et al. (2021)
42 ka–33 ka	western/central Europe	0.0006–0.0025	total area of calculation	Schmidt & Zimmerman (2019)
Late Palaeolithic (14 ka–11.7 ka)	Europe	0.0109	core area	Schmidt et al. (2020)

Late Palaeolithic (14 ka–11.7 ka)	Europe	0.0012–0.0042	total area of population	Schmidt et al. (2020)
20 ka–10 ka	Europe	0.0004–0.0200	'demographic' estimate	Schmidt et al. (2020)
15 ka–10 ka	western/central Europe	0.007	'absolute' mean	Schmidt et al. (2020)
15 ka–10 ka	western/central Europe	0.0030–0.0035	'absolute' median	Schmidt et al. (2020)
15 ka–10 ka	western/central Europe	0.0020–0.0025	'absolute' linear	Schmidt et al. (2020)
30 ka–13 ka	Europe	0.028–0.051	mean density	Tallavaara et al. (2015)
15 ka–13 ka	Greece	0.06–0.23	mean density	Tallavaara et al. (2015)

Fig. S4. Average annual rainfall (mm; orange-purple scale) pattern in Cyprus derived from the Climate Hazards Center InfraRed Precipitation with Station Data (CHIRPS) dataset from 1981–2022 (chc.ucsb.edu/data/chirps). Background blue indicates relative bathymetry.

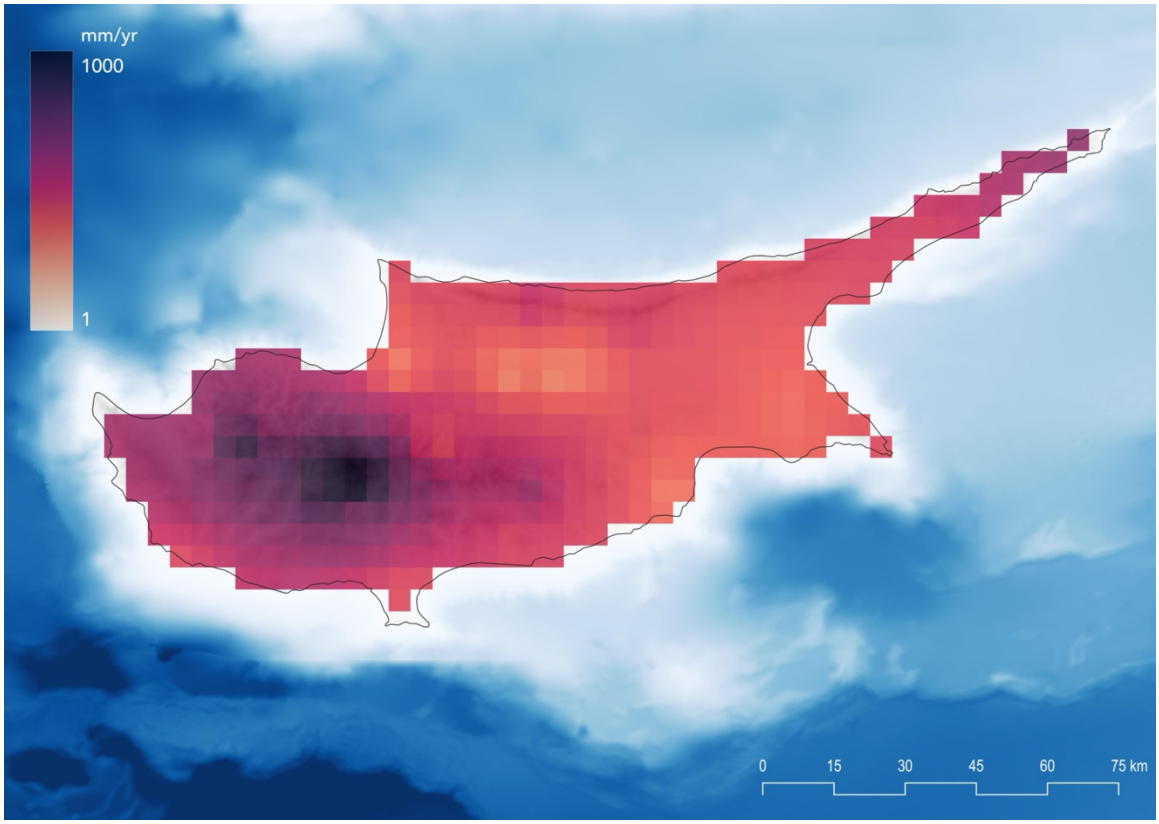

Fig. S5. Global sea-level variation (from 13) and reconstructed time series of Cyprus land area derived from the General Bathymetric Chart of the Oceans (gebco.net). Also shown are the calibrated re-sampled inverse-weighted McInerney (CRIWM) estimate of initial entry window (grey shading), the end of the Last Glacial Maximum (LGM; light blue shading), the Bølling-Allerød interstadial (B-O; light pink shading), the Younger Dryas (YD; light blue shading), and the early Holocene (brown shading).

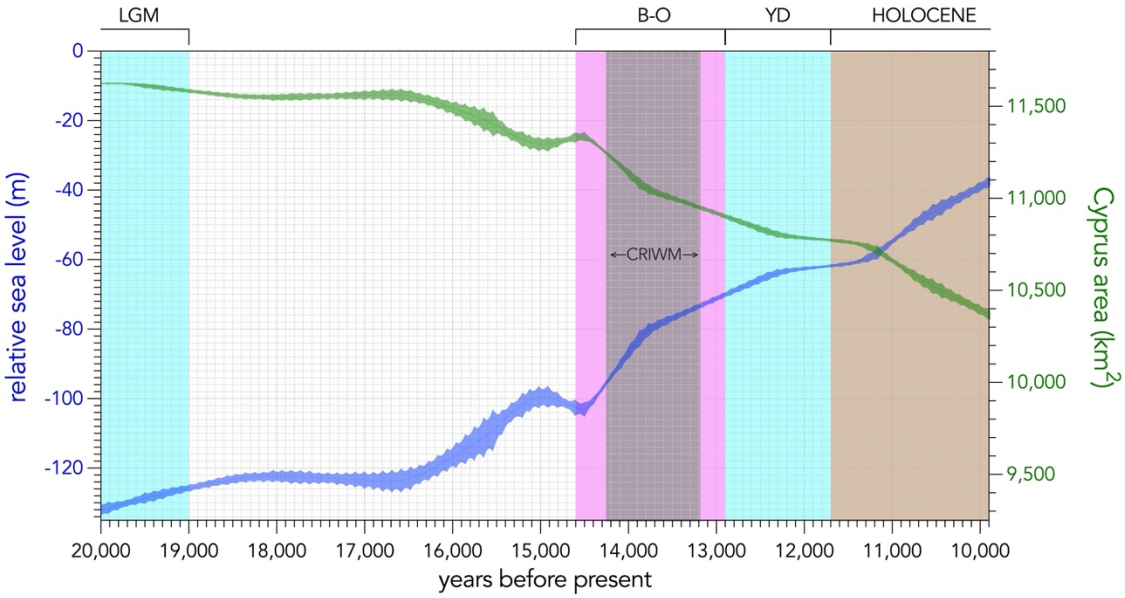

Fig. S6. An example projection of carrying capacity (*K*) based on the changing net primary production from the HadCM3 model (1) and size of Cyprus (changing with seal level; Fig. S5). Also shown are the calibrated re-sampled inverse-weighted McInerney (CRIWM) estimate of initial entry window (grey shading), the duration of the Younger Dryas (YD; light blue shading) and the early Holocene (brown shading).

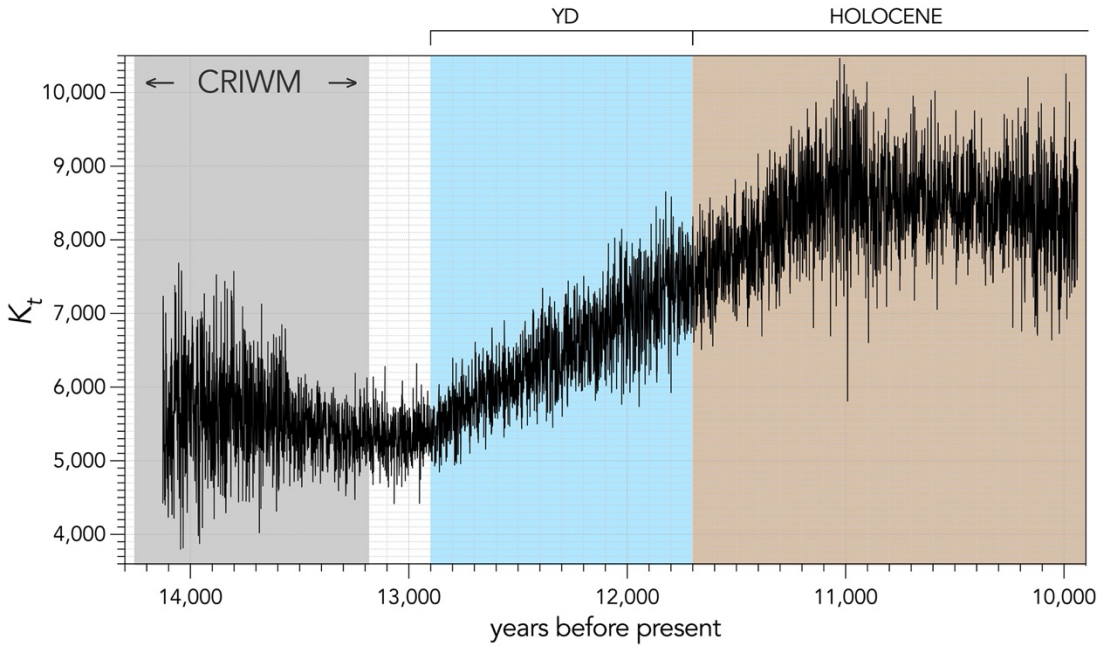

Appendix II

There is a single site (Vretsia *Roudias*) southwest of the Troodos Mountains for which optically stimulated luminescence dates exist, the oldest of which is 12.8 ± 1.6 ka (14). Incorporating this date into the calibrated chronology derived from the radiocarbon dates of the 10 oldest sites and re-applying the CRIWM Signor-Lipps correction pushes back the estimated window of initial human arrival by > 1700 years: 15.964–13.155 ka (*cf*. the radiocarbon-only window = 14.257–13.182 ka). The wider window occurs mainly because of the higher uncertainty of the optically stimulated luminescence date (1.6 ka) compared to those estimated from the radiocarbon dates (standard deviations: 0.281 to 0.023 ka).

SI References

1. Krapp M, Beyer RM, Edmundson SL, Valdes PJ, & Manica A (2021) A statistics-based reconstruction of high-resolution global terrestrial climate for the last 800,000 years. *Sci Dat* 8(1):228. doi:10.1038/s41597-021-01009-3
2. Liu Z*, et al.* (2009) Transient simulation of Last Deglaciation with a new mechanism for Bølling-Allerød warming. *Science* 325(5938):310-314. doi:10.1126/science.1171041
3. Liu Z*, et al.* (2014) Evolution and forcing mechanisms of El Niño over the past 21,000 years. *Nature* 515(7528):550-553. doi:10.1038/nature13963
4. Fordham DA*, et al.* (2017) PaleoView: a tool for generating continuous climate projections spanning the last 21 000 years at regional and global scales. *Ecography* 40(11):1348-1358. doi:10.1111/ecog.03031
5. Lundström V, Peters R, & Riede F (2021) Demographic estimates from the Palaeolithic–Mesolithic boundary in Scandinavia: comparative benchmarks and novel insights. *Phil Trans R Soc B* 376(1816):20200037. doi:10.1098/rstb.2020.0037
6. Coward F & Dunbar RIM (2014) Communities on the edge of civilization. *Lucy to Language: The Benchmark Papers*, (Oxford University Press, Oxford, United Kingdom), pp 380–406.
7. Binford LR (2001) *Constructing Frames of Reference: An Analytical Method for Archaeological Theory Building Using Ethnographic and Environmental Data Sets* (University of California Press, Berkeley).
8. Schmidt I*, et al.* (2020) Approaching prehistoric demography: proxies, scales and scope of the Cologne Protocol in European contexts. *Phil Trans R Soc B* 376(1816):20190714. doi:10.1098/rstb.2019.0714
9. Tallavaara M, Luoto M, Korhonen N, Järvinen H, & Seppä H (2015) Human population dynamics in Europe over the Last Glacial Maximum. *Proc Natl Acad Sci USA* 112(27):8232-8237. doi:10.1073/pnas.1503784112
10. Kavanagh PH*, et al.* (2018) Hindcasting global population densities reveals forces enabling the origin of agriculture. *Nat Hum Behav* 2(7):478-484. doi:10.1038/s41562-018-0358-8
11. Bocquet-Appel J-P, Demars P-Y, Noiret L, & Dobrowsky D (2005) Estimates of Upper Palaeolithic meta-population size in Europe from archaeological data. *J Archaeol Sci* 32(11):1656-1668. doi:10.1016/j.jas.2005.05.006
12. Schmidt I & Zimmermann A (2019) Population dynamics and socio-spatial organization of the Aurignacian: Scalable quantitative demographic data for western and central Europe. *PLoS One* 14(2):e0211562. doi:10.1371/journal.pone.0211562
13. Lambeck K, Rouby H, Purcell A, Sun Y, & Sambridge M (2014) Sea level and global ice volumes from the Last Glacial Maximum to the Holocene. *Proc Natl Acad Sci USA* 111(43):15296-15303. doi:10.1073/pnas.1411762111
14. Tsakalos E, Efstratiou N, Bassiakos Y, Kazantzaki M, & Filippaki E (2021) Early Cypriot prehistory: on the traces of the last hunters and gatherers on the island—preliminary results of luminescence dating. *Curr Anthropol* 62(4):412-425. doi:10.1086/716100